Uncoupled axial, flexural, and circumferential pipe-soil interaction analyses of partially supported jointed water mains

Rajani, B. B.; Tesfamariam, S.

Publisher's version / Version de l'éditeur:
https://doi.org/10.1139/T04-048
Canadian Geotechnical Journal, 41, December 6, pp. 997-1010, 2004-12-01

Uncoupled axial, flexural, and circumferential pipe–soil interaction analyses of partially supported jointed water mains

Balvant Rajani and Solomon Tesfamariam

Abstract: Pipelines used in the distribution of potable water are a vital part of everyday life. The pipelines buried in soil–backfill are exposed to different deleterious reactions; as a result, the design factor of safety may be significantly degraded and, consequently, pipelines may fail prematurely. Proactive pipeline management, which entails optimal maintenance, repair, or replacement strategies, helps increase the longevity of pipelines. The effect of different deterioration mechanisms and operating conditions needs to be understood to develop good proactive management practices. In this paper, a Winkler-type analytical model is developed to quantify the contributions of different stress drivers, e.g., pipe material type and size, bedding conditions, and temperature. Sensitivity analyses indicate that the extent of the unsupported length developed as a result of scour has a significant influence on the flexural pipe–soil response. As well, plastic pipes tolerate less loss of support than metallic pipes.

Key words: jointed water mains, Winkler model, pipe–soil interaction, elastoplastic soil.

Résumé : Les conduites utilisées pour la distribution de l'eau potable constituent une partie vitale de la vie de tous les jours. Les conduites enfouies dans un remblai de sol sont exposées à différentes réactions nuisibles, et il en résulte une dégradation du coefficient de sécurité utilisé pour le calcul et en conséquence les conduites se brisent prématurément. La gestion proactive des conduites qui comporte des stratégies optimales de maintenance, de réparation, ou de remplacement aide à accroître la longévité des conduites. L'effet de différents mécanismes de détérioration et conditions d'opération doit être bien compris de façon à développer de bonnes pratiques de gestion proactive. Dans cet article, on a développé un modèle analytique de type Winkler pour quantifier les contributions de différentes sources de contraintes, e.g., type de matériau et dimension de la conduite, conditions du coussin, et température. Des analyses de sensibilité indiquent que l'importance de la longueur non supportée qui se développe à la suite de l'érosion a une influence significative sur la réaction conduite–sol en flexion. Également, les conduites en plastique tolèrent moins de perte d'appui que les conduites métalliques.

Mots clés : conduites maîtresses d'eau articulées, modèle Winkler, interaction sol–conduite, sol élasto-plastique.

[Traduit par la Rédaction]

Introduction

Understanding failure mechanisms of deteriorating infrastructure is paramount for the proactive management of infrastructure assets. Exposure of water mains to aggressive environmental conditions and deleterious reactions can lead to significant deterioration so as to undermine their ability to reliably deliver safe drinking water. The life cycle of a typical buried pipe is described by the so-called "bathtub" curve as shown in Fig. 1. It describes the instantaneous failure probability (hazard function), and the bathtub curve often distinguishes between three phases in the life of a pipe. The first phase, also known as the "burn-in" phase, describes the period right after installation, in which breaks occur mainly as a result of faulty installation or faulty pipes. These breaks emerge gradually and are fixed in a declining frequency. Once the system is purged of these "early" problems, the pipeline enters phase two, in which the pipe operates relatively trouble free, with a low failure frequency resulting from random phenomena such as unusual heavy loads and third-party interference. The third phase, also called the "wear-out phase," depicts a period of increasing failure frequency due to pipe deterioration and ageing. Not every pipe experiences every phase, and the length of the phases may vary dramatically for various pipes and under various conditions. Alternatively, the various phases in the deterioration of structural reliability (expressed here as the factor of safety) that ultimately lead to the failure of the water main are shown in Fig. 2. Older water mains are usually made of pit- or spun-cast iron (CI), and the newer mains are largely made of ductile iron (DI) or polyvinyl chloride (PVC). In an aggressive environment, corrosion in CI takes the form of graphitization (Makar and Rajani 2000), and pitting takes place in DI pipes. PVC water mains have not been used long enough to establish a definite deterioration mechanism.

Received 26 August 2003. Accepted 13 April 2004. Published on the NRC Research Press Web site at http://cgj.nrc.ca on 29 October 2004.

B. Rajani[1] and S. Tesfamariam. Institute for Research in Construction, National Research Council Canada, Ottawa, ON K1A 0R6, Canada.

[1]Corresponding author (e-mail: Balvant.Rajani@nrc-cnrc.gc.ca).

 doi: 10.1139/T04-048

Fig. 1. The "bathtub" curve of the life cycle of a buried pipe.

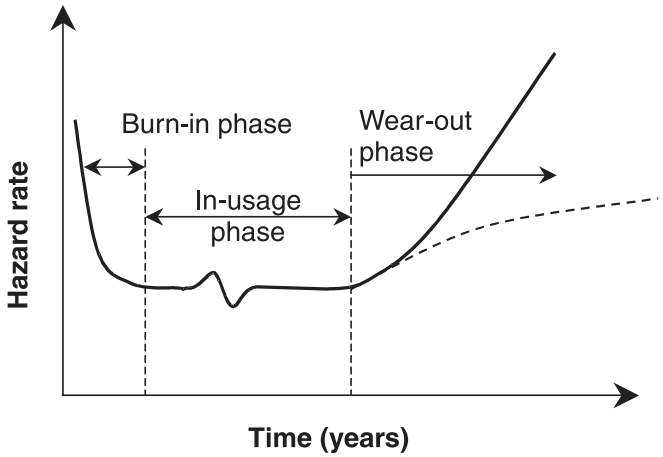

Fig. 2. Decrease in factor of safety with time.

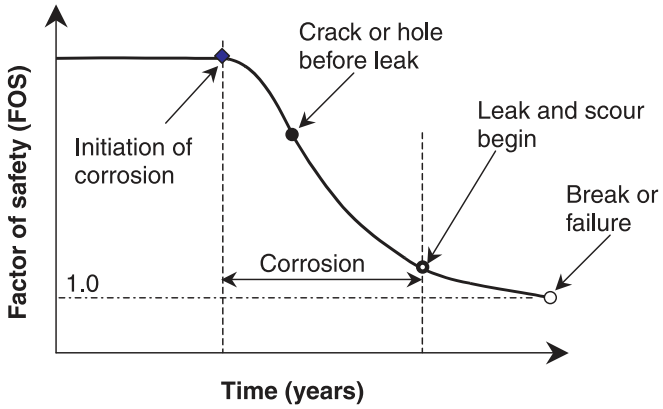

Nonetheless, whatever the pipe materials and the associated deterioration mechanisms, it is assumed that structural strength will decrease, say, as a consequence of corrosion pitting, graphitization, fracture, creep, or material softening. It is further assumed that a leak will develop as soon as the pipe wall is breached. The leak will in turn scour the surrounding bedding and undermine the soil support to the pipe. The size of the corrosion pit and the extent to which the bedding support is lost ("unsupported" length) will lower the design factor of safety. An arch is likely to form in sandy soils (backfills); if the leak occurs at the pipe invert or crown, analysis is not required because the pipe is not loaded. A leak at the crown in clayey soils is likely to unload the pipe initially, but as the soil becomes saturated the clay is likely to cave in and impose earth loads on the pipe. On the other hand, the proposed model allows for any load (q) on the unsupported pipe length, i.e., if arching merits consideration, then the load can be reduced. Consequently, the model considers what can be referred to as a "worst-case" scenario.

Three ingredients required to develop frost heave and hence frost load are availability of water, thermal gradient, and soil with appropriate particle size and hence pore size (Rajani and Zhan 1996). The presence of a water main leak contributes to the first of the three ingredients. All three lead to increased stresses on the pipe which were not considered in the original structural design when the pipes were installed years ago. Rajani et al. (1996), in analyzing pipe breakage, did not include an assessment of the influence of unsupported length, which could result as a consequence of water leaks and possible shrinkage due to moisture changes in bedding materials. In most cases, shrinkage-susceptible native material (predominantly clayey and silty soils in most urban areas in Canada) was used as backfill and as bedding material for CI pipe installations.

Water mains used in water distribution systems have bell and spigot connections and are referred to here as jointed pipes; typical pipe lengths are 6 m (20 ft). Elastomer gaskets at bell and spigot connections (joints) prevent leaks while permitting axial movement and slight rotation (3–4°) to accommodate limited movement of soil bedding. In the analysis described here, boundary conditions dictated by a bell–spigot joint are assumed to be ideal, i.e., free to move longitudinally and permit rotation. In practice, these movements are likely to be restrained as a consequence of ageing of both pipe joint and gasket materials. Longitudinal and rotational movements are probably restrained to a greater extent in the case of cast iron pipes than for modern pipe materials. Structural design of water mains usually provides sufficient (with an accepted margin of safety) resistance against circumferential (in-plane) stresses imposed by soil overburden loads, live traffic loads, and internal pressure. Loads imposed on pipes as a result of temperature changes, soil pressures induced by frost heave, and loss of support from bedding are largely unaccounted for in the axial, flexural (longitudinal bending), or circumferential response analyses. The practice to exclude some of these circumstances from routine analyses and design is acceptable as long as the margin of safety is adequate and pipes do not deteriorate with time, leak, and develop locations with loss of bedding support or differential settlement. Ageing water distribution systems, however, do indicate that pipes deteriorate with time and that there is a marked increase in the number of water main breaks with dramatic temperature differentials between the water in the pipe (1–2 °C) and the adjacent soil (10–12 °C).

The intent of this paper is to quantify the impact of the unsupported length and soil elastoplasticity on the axial and flexural responses considering pipe–soil interaction using the Winkler model. Further, the axial, flexural, and circumferential stress components are consolidated from the analyses described here, and previously reported (Rajani et al. 1996; Ugural and Fenster 1987), to provide an overall picture of the response of buried water mains under the influence of earth and live loads, water pressure, temperature differential, and pipe–soil interaction. Though the extent of loss of support cannot be determined in the field today, several attempts have been made by Makar (1999) for sewers using nondestructive techniques.

The axial and flexural responses of buried jointed pipe is considered to be uncoupled, and it is assumed that the pipe deformations are small and always within the elastic range. For simplicity, it is also assumed that the leak produces scour (undermined bedding) at the centre of jointed pipe of length $2L$, probably representing a worst-case scenario. The soil or bedding in the pipe–soil interaction analysis is considered as an elastoplastic Winkler model. Generally, the Winkler model has several shortcomings, e.g., it assumes no

interaction through the soil from location to location and no interaction through shear nor volumetric effects, and the model relies on a definition of soil pressure in terms of absolute displacement of the pipe, not the displacement of the pipe relative to the soil. Nevertheless, given all uncertainties in modelling pipe–soil interaction, it is an acceptably simple model to permit the consideration of axial effects, longitudinal bending and radial effects associated with overburden pressures, internal pressure, frost loads, and thermal effects. It is important to note that the circumferential response corresponds to that of a rigid pipe but could easily be extended to that of a flexible pipe. This consideration is appropriate for the pipe materials (CI and DI) and pipe sizes of interest here. In the analysis that follows it is assumed that thrust is positive when it results in tensile stresses in the pipe wall and negative when it results in compressive stresses. Similarly, a moment (longitudinal bending) is positive when there are tensile stresses on the pipe invert and negative when there are compressive stresses on the pipe invert. Tensile stresses in the circumferential direction are treated as positive.

Typical pipe–soil systems are considered in the sensitivity analyses to illustrate the applicability of the proposed models. Pipe and soil properties and the operating conditions selected in these analyses are typical of those likely to be encountered in practice.

Axial pipe–soil interaction

Rajani et al. (1996) described the Winkler model for axial pipe–soil interaction of a jointed buried pipe in an elastic soil (medium). The equilibrium equation is governed by

$$[1] \qquad \frac{\partial \sigma_x^a}{\partial x} - \frac{k_s^a}{t} u = 0 \qquad u < u_x$$

where σ_x^a is the axial stress, u is the axial displacement, k_s^a is the axial pipe–soil reaction modulus, t is the pipe wall thickness, and u_x is the displacement required to develop ultimate axial resistance (Committee on Gas and Liquid Fuel Lifelines 1984). The axial pipe–soil reaction modulus of the soil can be estimated using the elastic properties as suggested by Scott (1981) or empirical relationships for sand and clay as suggested by the Committee on Gas and Liquid Fuel Lifelines (1984). These relationships are as follows:

$$[2a] \qquad k_s^a = \frac{G_s}{4(1-\upsilon_s)D/2} \qquad \text{elastic soil}$$

$$[2b] \qquad k_s^a = \frac{\alpha s_u}{u_x} \qquad u_x = 2.5 - 10.0 \text{ mm for clay}$$

$$[2c] \qquad k_s^a = \frac{0.5(\gamma_s H)(1+K_o)\tan\delta}{u_x}$$

$$u_x = 2.5 - 5.0 \text{ mm for sand}$$

where D is the external diameter of the pipe, G_s is the soil shear modulus, υ_s is the soil Poisson's ratio, α is the adhesion coefficient, s_u is the undrained shear strength of clay, γ_s is the submerged unit weight, H is the burial depth of water mains from the surface to the centreline of the pipe, K_o is the coefficient of active resistance at rest, and δ is the frictional angle between the pipe material and the surrounding backfill.

Fig. 3. Typical axial soil resistance versus axial displacement.

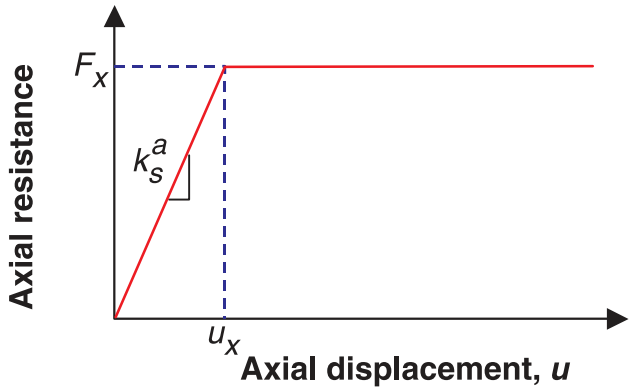

If the soil is represented as an elastoplastic material (Fig. 3) and the soil deformation exceeds the limiting axial displacement, $u = u_x$, then the governing equilibrium equation is

$$[3] \qquad \frac{\partial \sigma_x^a}{\partial x} - \frac{F_x}{t} = 0 \qquad u \geq u_x$$

where F_x is the ultimate axial resistance and is given by

$$[4] \qquad F_x = k_s^a u_x$$

Equations [1] and [3] are applicable to a pipe that is fully supported longitudinally and radially (normal to the circumferential direction). As discussed earlier, the bedding of a leaky pipe is likely to be scoured, causing the pipe to lose support. This situation necessitates that the problem be solved piece-wise in three regions, i.e., unsupported pipe length (b), pipe embedded in an elastic soil (d), and remaining pipe length in plastic soil (f) (Fig. 4). The soil is represented as a Winkler elastoplastic material.

The axial response (solution to eq. [1]) of the supported pipe length d is described by

$$[5] \qquad u_d = C_1^a \exp(-\gamma x_d) + C_2^a \exp(+\gamma x_d)$$

where u_d is the axial displacement of the pipe embedded in the elastic soil; C_1^a and C_2^a are axial pipe–soil interaction constants; and γ is the reciprocal of the axial characteristic length, given by

$$[6] \qquad \gamma^2 = \frac{k_s^a}{E_p t\{[1+\upsilon_p^2 E_s/2\beta_l(1+\upsilon_s)E_p](1+D/t)\}}$$

where υ_p is Poisson's ratio of the pipe, β_l is a constant as defined in Rajani et al. (1996), E_s is the elastic modulus of the soil, and E_p is the elastic modulus of the pipe.

The axial response of the portion of the pipe supported by elastoplastic soil is given by

$$[7] \qquad u_f = \frac{F_x x_f^2}{2tE_p} + F_1^a x_f + \alpha_p \Delta T x_f + F_2^a$$

where u_f is the axial displacement of the pipe embedded in the elastoplastic soil, E_p is the pipe elastic modulus, and F_1^a and F_2^a are constants. Temperature change in the soil is cap-

Fig. 4. Schematic model for axial and radial pipe–soil interaction.

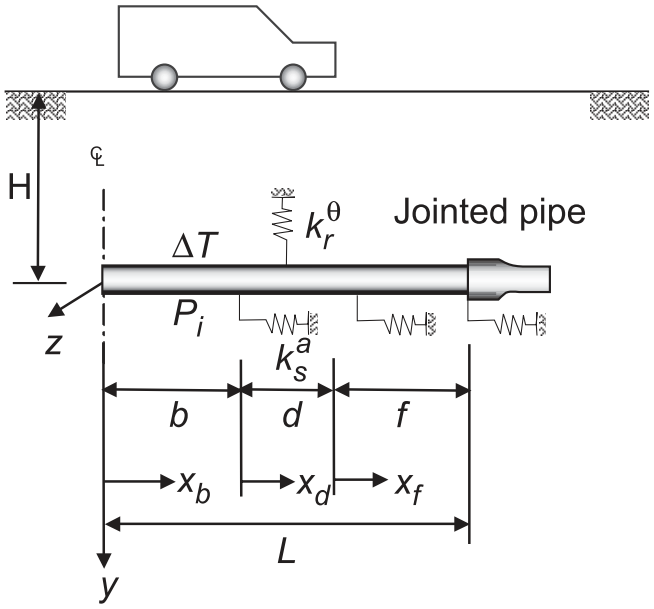

tured by the term $\alpha_p \Delta T x_f$, where α_p is the linear thermal expansion coefficient of the pipe material, ΔT is the maximum temperature difference between the water and the surrounding soil, and x_f is the longitudinal coordinate system for soil in plastic region (Fig. 4).

Similarly, the unsupported pipe length b is an axially loaded prismatic element, and its response is described by

$$[8] \quad u_b = B_1^a x + \alpha_p \Delta T x_b + B_2^a$$

where u_b is the axial displacement of the unsupported pipe, B_1^a and B_2^a are constants, and x is the distance along the pipe from the centreline. Symmetry considerations require that $u_b(x = 0) = 0$, and consequently $B_2^a = 0$ because unsupported length is assumed to form at the centre of the pipe segment. The other boundary conditions are essentially compatibility requirements for deformations at transition points from portions of pipe within different regions of soil behaviour, i.e., $u_b(x_b = b) = u_d(x_d = 0)$, $u_b'(x_b = b) = u_d'(x_d = 0)$, $u_d(x_d = d) = u_f(x_f = 0)$, $u_d'(x_d = d) = u_f'(x_f = 0)$, and $\sigma_x^a(x_f = f) = 0$, where σ_x^a is the axial stress. The unknown constants B_1^a, C_1^a, C_2^a, F_1^a, and F_2^a can be obtained by applying these boundary conditions:

$$[9] \quad B_1^a = \frac{-2F_x d}{t\chi_4} + \frac{\chi_5\chi_2}{\chi_4} P_i - \frac{\chi_6}{\chi_4} E_p \alpha_p \Delta T$$

$$[10] \quad C_1^a = \frac{B_1^a}{E_p}\left(\frac{b}{2} - \frac{1}{2\gamma\chi_1}\right) + \frac{P_i}{E_p}\left(\frac{\chi_2}{2\gamma\chi_1}\right) + \alpha\Delta T\left(\frac{b}{2} - \frac{\chi_3}{2\gamma\chi_1}\right)$$

$$[11] \quad C_2^a = \frac{B_1^a}{E_p}\left(\frac{b}{2} + \frac{1}{2\gamma\chi_1}\right) - \frac{P_i}{E_p}\left(\frac{\chi_2}{2\gamma\chi_1}\right) + \alpha\Delta T\left(\frac{b}{2} + \frac{\chi_3}{2\gamma\chi_1}\right)$$

$$[12] \quad F_1^a = \frac{-F_z f}{t}$$

$$[13] \quad F_2^a = C_1^a \exp(-\gamma d) + C_2^a \exp(+\gamma d)$$

where χ_1, χ_2, and χ_3 are as defined by Rajani et al. (1996) to account for axial pipe movement, internal water pressure, and temperature change, respectively; P_i is the internal water pressure; α_p is the linear thermal expansion coefficient of the pipe material; and F_z is the maximum lateral soil resistance per unit length. The constants χ_4, χ_5, and χ_6 are as follows:

$$[14a] \quad \chi_4 = (1 + b\gamma\chi_1)\exp(\gamma d) + (1 - b\gamma\chi_1)\exp(-\gamma d)$$

$$[14b] \quad \chi_5 = -2 + \exp(\gamma d) + \exp(-\gamma d)$$

$$[14c] \quad \chi_6 = -2\chi_3 + (b\gamma\chi_1 + \chi_3)\exp(\gamma d) - (b\gamma\chi_1 - \chi_3)\exp(-\gamma d)$$

The axial stress responses in the three different regions of soil behaviour can be expressed in terms of "stress drivers," i.e., axial pipe movement, internal water pressure, and temperature change:

$$[15a] \quad \sigma_x^a = \frac{F_x}{t}(x_f - f) \quad \text{for} \quad (b + d) \le x < (b + d + f)$$

$$[15b] \quad \sigma_x^a = \chi_1 E_p \frac{\partial u_d}{\partial x} + \chi_2 P_i - \chi_3 E_p \alpha_p \Delta T \quad \text{for} \quad b \le x < (b + d)$$

$$[15c] \quad \sigma_x^a = \frac{-2F_x d}{t\chi_4} + \frac{\chi_5\chi_2}{\chi_4} P_i - \frac{\chi_6}{\chi_4} E_p \alpha_p \Delta T \quad \text{for} \quad 0 \le x < b$$

where σ_x^a is the axial stress. If the soil yields beyond the plastic limit, i.e., $u_d > u_x$, the temperature change will not have any influence on the axial stress as shown by eq. [15*a*].

This solution is similar to that developed by Rajani et al. (1996) except that the soil supporting medium is considered as elastoplastic and there is an added consideration for the loss of bedding support as a consequence of scour developed from a leaky pipe. The solution reverts to that previously obtained by Rajani et al. (1996) when the unsupported length, b, is zero and the soil is elastic.

Sensitivity analyses: axial stress

A sensitivity analysis was carried out to investigate the axial response of buried pipe to different pipe materials, pipe diameters, soil types, and soil temperatures close to the pipe. A 150 mm (6 in.) CI pipe buried in medium sand with k_s^a = 125 MPa/m was selected as a reference case (Table 1) to gauge the sensitivity of the axial pipe–soil system to variations of different parameters.

Table 1. Reference data for typical cast iron (CI), ductile iron (DI), and polyvinyl chloride (PVC) water mains, soil properties, and operating conditions.

(A) Reference data for pipe material			
	CI	DI	PVC
Pipe diameter (mm)	150 (6 in.)	100 (4 in.)	200 (8 in.)
External diameter, D (mm)	175.26	121.92	229.87
Wall thickness, t (mm)	10.92	10.16	10.16
Pipe length, $2L$ (m)	6.0	6.0	6.0
Elastic modulus, E_p (MPa)	206 000	165 000	2250
Ultimate tensile strength (MPa)	207	290	48
Poisson's ratio, υ_p	0.26	0.28	0.42
Thermal coefficient, α_p ($\times 10^{-6}$/°C)	10.5	11.0	79.0
(B) Soil properties			
	Medium sand	Very soft clay	
Elastic modulus, E_s (MPa)	100	1.5	
Poisson's ratio, υ_s	0.3	0.3	
Soil unit density, ρ (kg/m^3)	2344	1988	
Lateral foundation modulus, k_s' (MPa)	50		
Axial foundation modulus, k_s^a (MPa/m)	125		
(C) Operating conditions			
Water pressure, P_i (kPa)	345 (50 psi)		
Installation temperature (°C)	24		
Temperature amplitude, A_T (°C)	15		
Annual mean temperature (°C)	15		
Overburden load, q (N/mm)	27.13		
Frost load factor, f_{frost}	0.5		

The axial stress profile for a 150 mm diameter CI main shown in Fig. 5 indicates that the axial stress decreased as the unsupported length increased, since the pipe length that is constrained from movement decreases. Similar responses are observed as unsupported pipe lengths increase and pipe diameters decrease (Fig. 6) or if the soil temperatures close to the pipe decrease (Fig. 7). Axial stresses induced at the pipe–soil interface will be lower in large-diameter pipes because of a proportional increase in contact surface area. This is expected because the remaining pipe length that is subjected to axial restraint decreases as the unsupported pipe length increases.

Figure 8 shows the maximum axial stress (expressed as a percentage of the ultimate tensile strength) induced in different pipe materials (CI, DI, and PVC) as a consequence of temperature differential (between soil temperature and temperature of water in the pipe). Although there are no appreciable differences between the axial responses of CI and DI pipes, the PVC pipe shares a significant proportion (7% of the ultimate stress at ΔT of –14 °C) of the stress because of its higher thermal expansion coefficient and lower elastic modulus.

Axial stresses in the pipe increase (Fig. 9) as the soil becomes stiffer, i.e., higher axial foundation moduli, for any specific unsupported pipe length. As explained earlier, this increase is accentuated at shorter unsupported lengths because more of the pipe surface in contact with the soil is restrained. The role of elastoplastic behaviour of the soil shown in Fig. 10 corresponds to a pipe with an unsupported length of b = 500 mm and clearly illustrates that consideration of elastoplasticity increases the axial stresses induced in the pipe compared with elastic analysis only. Elastoplastic response of the soil was artificially induced in this example by increasing the temperature difference (–56 °C) by four times the value (–14 °C) used in the rest of analyses to illustrate the fact that a large temperature differential would have to exist to induce significant stress.

Flexural pipe–soil interaction

A pipe buried at constant depth in soil backfill or bedding with uniform geotechnical properties should not be normally subjected to flexural or bending deformations or stresses in the longitudinal direction. Loss of bedding support near the pipeline under circumstances described earlier, however, subjects the pipe to flexural stresses. The total load, q, imposed on the unsupported length of the pipe is the earth load together with the traffic and frost loads. The soil near the unsupported pipe region may exceed the elastic displacement limit (v_u) and develop plastic deformations if the overburden loads or unsupported length are high enough. Prior to the development of solutions for a jointed pipe, simple solutions considering the supported portion of the pipe as an infinite beam (when $\lambda[L - (b + c)] > \pi$, where λ is the reciprocal of the flexural characteristic length as defined in eq. [18]) on an elastoplastic foundation (Fig. 11) were obtained to determine if there was merit to incorporating soil elastoplasticity. These simple solutions indicated that soil elastoplasticity is significant for typical pipe–soil characteristics encountered in the water distribution systems when the unsupported

Fig. 5. The effect of unsupported length, b, on axial stress.

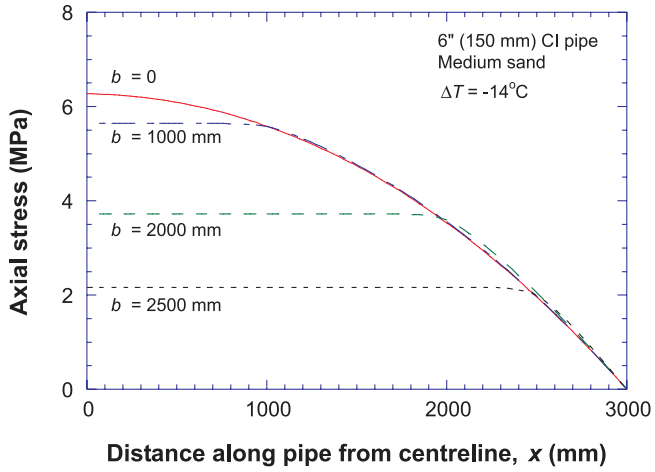

Fig. 6. The effect of pipe size and unsupported length on axial stress.

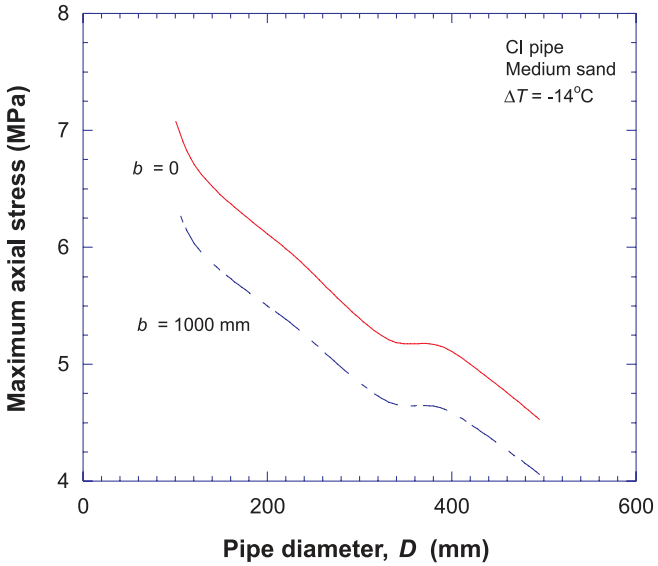

length is greater than 2 m and rigid body movement is permitted. Thus, two distinct regions of soil in contact with the pipe can be characterized as plastic and elastic, where x_c and x_e represent the coordinate axes of regions c and e, respectively, in Fig. 11. The pipe in these circumstances can be modelled as a beam on an elastoplastic foundation (bepf) with partial support.

Frost load (Rajani and Zhan 1996) can be accounted for in a simple form as a multiple of the frost load factor (f_{frost}) of the soil load. The frost load multiple, f_{frost}, ranges from 1, where there is no frost load, to 2, the maximum expected frost load.

The equilibrium equation for the portion of the pipe supported by elastic bedding is represented by a Winkler beam on an elastic foundation (bef) (Hetényi 1946):

$$[16] \quad E_{\text{p}} I_{zz} \frac{\mathrm{d}^4 v_e}{\mathrm{d}x^4} + k_{\text{s}}' v_e = 0$$

Fig. 7. The effect of seasonal pipe temperatures on axial stress.

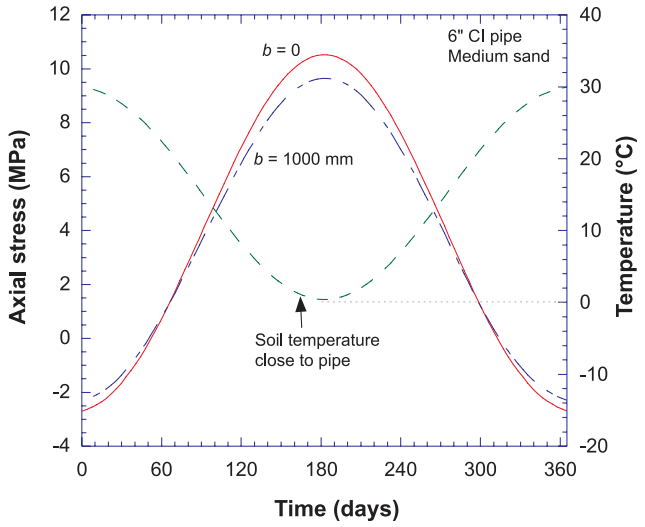

Fig. 8. The effect of pipe material on axial stress as a result of temperature difference.

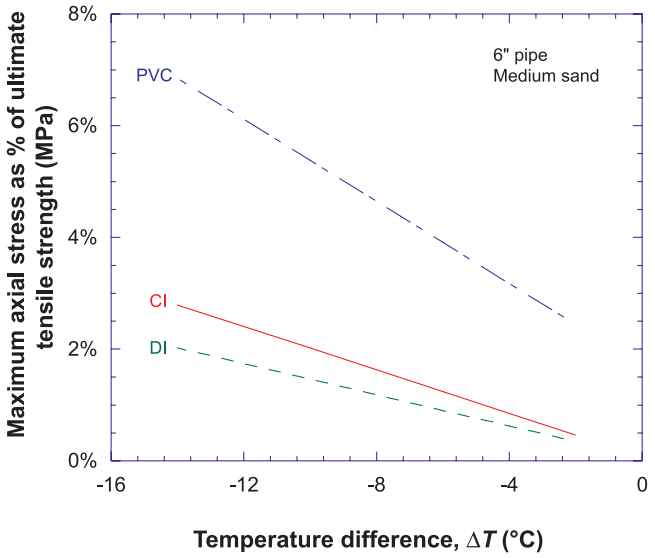

where I_{zz} is the second moment of inertia of the pipe around the z axis, v_e is the pipe vertical displacement in the elastic soil region, and k_{s}' is the lateral elastic foundation modulus of the soil. The general solution for v_e is

$$[17] \quad v_e = \exp(\lambda x_e)(E_1 \cos \lambda x_e + E_2 \sin \lambda x_e) + \exp(-\lambda x_e)(E_3 \cos \lambda x_e + E_4 \sin \lambda x_e)$$

where E_1, E_2, E_3, and E_4 are constants; and the reciprocal of λ is the reciprocal of the flexural characteristic length:

$$[18] \quad \lambda = \sqrt[4]{\frac{k_{\text{s}}'}{4E_{\text{p}} I_{zz}}}$$

The lateral elastic foundation modulus of the soil, k_{s}', in terms of elastic soil properties can be estimated as suggested by Vesic (1961):

Fig. 9. The effect of soil stiffness, k_s^a, and unsupported length on axial stress.

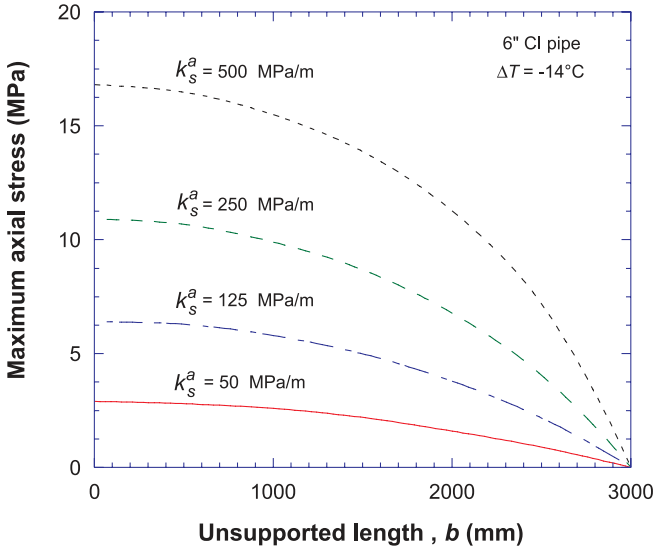

Fig. 10. The effect of elastoplastic analysis on axial stress.

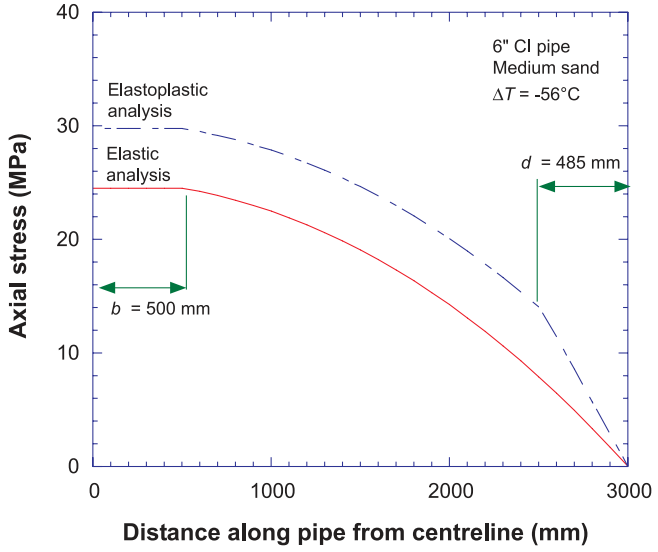

$$[19] \quad k_s' = \frac{0.65E_s}{1-\upsilon_s^2}\sqrt[12]{\frac{E_s D^4}{E_p I_{zz}}}$$

Differentiation of vertical displacement v with respect to x gives the slope, moment, and shear, respectively, as $v' = \tan\theta$, $-E_p I_{zz} v'' = M_x$, and $-E_p I_{zz} v''' = Q$, where θ is the slope, M_x is the bending moment, and Q is the shear force.

As stated earlier, loss of support is likely to induce soil deformations that are beyond the elastic limit, v_u, and hence will induce plastic deformations in the soil immediately adjacent to the point of lost support. The limiting elastic deformation, v_u, when the plastic deformations of the soil initiate (Fig. 12) is given by

$$[20] \quad v_u = F_z / k_s'$$

Fig. 11. Schematic model for partially supported pipe on elastoplastic foundation.

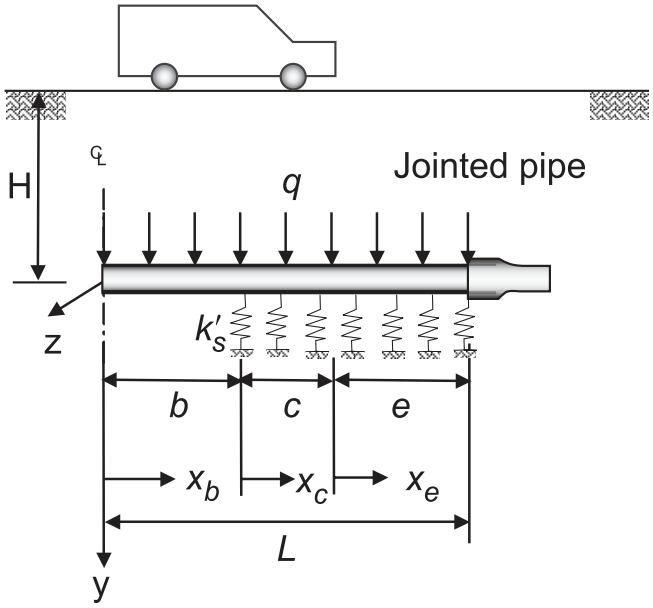

Fig. 12. Typical lateral soil resistance versus displacement.

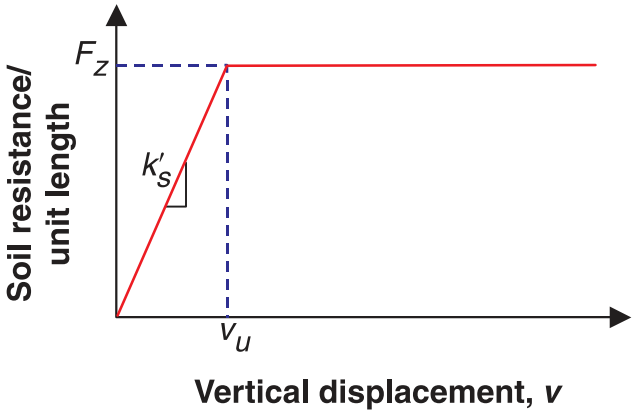

where F_z is the maximum lateral soil resistance per unit length.

The maximum lateral soil resistance per unit length, corresponding to the undrained state, is computed as proposed by Trautmann et al. (1985) and Poulos and Davis (1980) for sand and clay as follows:

$$[21] \quad F_z = \gamma_s D H N_z \quad \text{for} \quad \text{sand}$$

$$[22] \quad F_z = \bar{N}_c D s_u \quad \text{for} \quad \text{clay}$$

where N_z is a dimensionless resistance factor for sand, and $\bar{N}_c$ is the bearing capacity type factor.

The factor $\bar{N}_c$ depends on the ratio of burial depth (H) to pipe diameter (D). For typical pipe sizes and burial depths, the ratio H/D can vary between 3 and 20. Rowe and Davis (1982) have shown that the value of $\bar{N}_c$ (= 11.42) is essentially constant for $H/D > 3$. Using Vesic's equation, Das (1995) showed that N_z is approximately 18.4 when the angle of internal friction ϕ is 30°.

The equilibrium equation for the portion of the pipe embedded in soil with plastic deformations (region c in Fig. 11) is given by

$$[23] \quad E_p I_{zz} \frac{d^4 v_c}{dx^4} + F_z = 0$$

The displacement response, v_c, for the eq. [23] is

$$[24] \quad v_c = \frac{-F_z x_c^4}{24 E_p I_{zz}} + \frac{C_1 x_c^3}{6} + \frac{C_2 x_c^2}{2} + C_3 x_c + C_4$$

where C_1, C_2, C_3, and C_4 are constants.

The vertical deflection (v_b) along the unsupported length of the pipe subjected to a uniform load (soil and live), q, can be described by the fourth-order polynomial

$$[25] \quad v_b = \frac{q x_b^4}{24 E_p I_{zz}} + \frac{B_1 x_b^3}{6} + \frac{B_2 x_b^2}{2} + B_3 x_b + B_4$$

where B_1, B_2, B_3, and B_4 are constants.

It is assumed that there is no vertical movement at the bell–spigot joint relative to the adjacent jointed pipe and, as indicated earlier, bell–spigot joints permit rotation and hence no moment will develop. Therefore, the corresponding boundary conditions at the bell–spigot joint are $v_e(x_e = L) = 0$ and $v_e''(x_e = L) = 0$. Symmetry considerations at the centreline dictate the boundary conditions, zero rotation, $v_b'(x_b = 0) = 0$, and zero shear, $v_b'''(x_b = 0) = 0$. Consequently, B_1 and B_3 are equal to zero. At $x_b = b$ and $x_c = 0$, to satisfy continuity and compatibility, the boundary conditions are $v_b(x = b) = v_c(x_c = 0)$, $v_b'(x_b = b) = v_c'(x_c = 0)$, $v_b''(x_b = b) = v_c''(x_c = 0)$, and $v_b'''(x_b = b) = v_c'''(x_c = 0)$. Similarly, at $x_c = c$ and $x_e = 0$, to satisfy continuity and compatibility, the boundary conditions are $v_c(x_c = c) = v_e(x_e = 0)$, $v_c'(x_c = c) = v_e'(x_e = 0)$, $v_c''(x_c = c) = v_e''(x_e = 0)$, and $v_c'''(x_c = c) = v_e'''(x_e = 0)$. The unknowns in eqs. [17], [24], and [25] can be determined by applying these boundary conditions. Detailed derivations and descriptions of the unknown terms are given in Appendix A. The unknown terms of eq. [17], B_2, and B_4 are given in eqs. [26] and [27]:

$$[26] \quad B_2 = \frac{F_z c/2E_p I_{zz}\lambda^3 + qb/2E_p I_{zz}\lambda^3 + \theta_3 + \theta_2 + \alpha_6 - \alpha_4}{-\theta_4 - \theta_1 + \alpha_7 - \alpha_5}$$

$$[27] \quad B_4 = C_4 - \frac{q b^4}{24 E_p I_{zz}} - \frac{B_2 b^2}{2}$$

where α_4–α_7 and θ_1–θ_4 are constants.

Sensitivity analyses: flexural stress

A cursory look indicates that a number of variables influence the flexural response of a partially unsupported pipe on an elastoplastic bedding. Sensitivity analyses are carried out to identify the role of the principal variables such as soil type, pipe material, and pipe diameter. The same 150 mm (6 in.) CI pipe used for the sensitivity study of axial pipe–soil interaction is used to study the flexural pipe–soil interaction except that the lateral foundation modulus for medium sand is selected as $k_s' = 50$ MPa.

For a given unsupported length, two locations (Fig. 13) along the length of the pipe are susceptible to high stresses:

Fig. 13. The effect of pipe size and unsupported length on flexural stress.

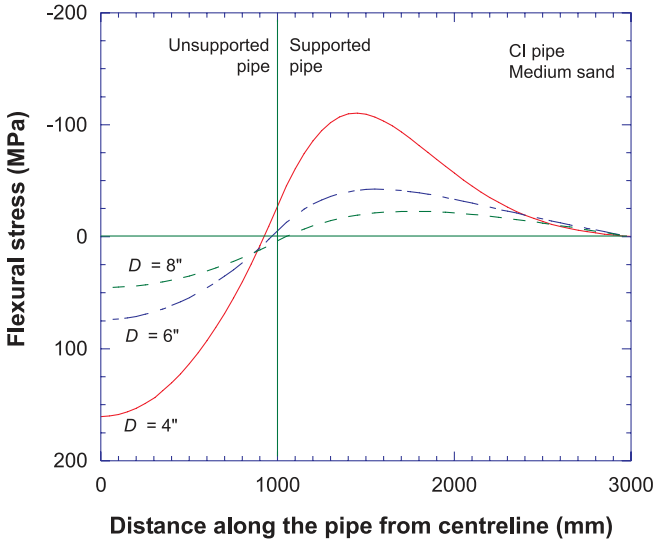

Fig. 14. The effect of pipe size and unsupported length on the maximum flexural stress.

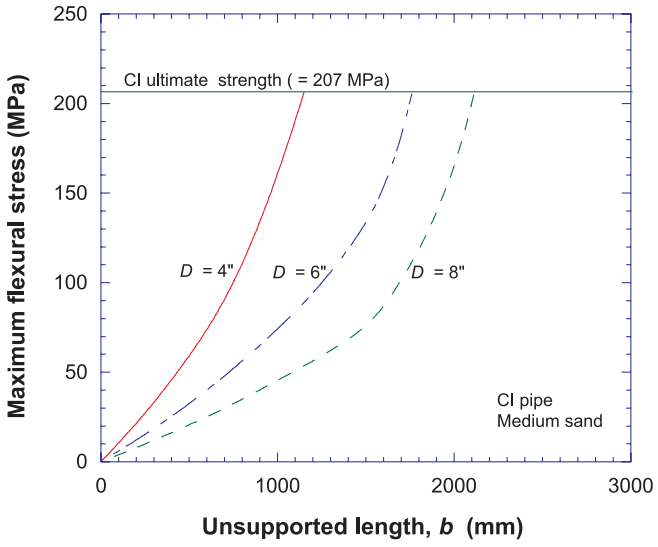

at the centreline and in the soil at the location where the pipe support ends. As expected, small-diameter mains experience higher stresses (Figs. 13, 14) than large-diameter mains, and the stress differences increase as the unsupported length, b, increases (Fig. 14). The 100 mm (4 in.), 150 mm (6 in.), and 200 mm (8 in.) diameter CI pipes approach ultimate strength at b = 1150, 1760, and 2180 mm, respectively.

The flexural stresses in CI and DI pipes are comparable (Fig. 15), as both pipes have higher moduli of elasticity than PVC. The 150 mm PVC, CI, and DI pipes approach their respective ultimate strengths (Fig. 16) at unsupported lengths of b = 1000, 1760, and 1880 mm. This highlights the fact that CI and DI pipes can tolerate much higher unsupported lengths than PVC pipes.

The lateral elastic foundation modulus of the soil, k_s', is influenced by the pipe rigidity, $E_p I_{zz}$, and elastic modulus of the soil. The foundation moduli, k_s', can range between 24

Fig. 15. The effect of pipe material and unsupported length on flexural stress.

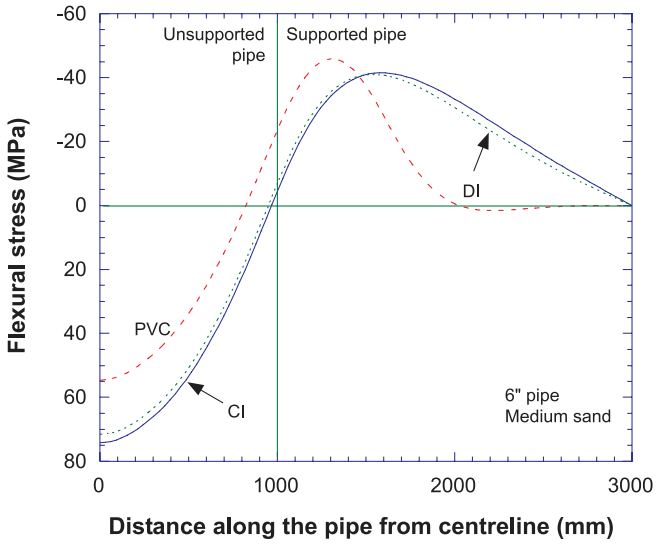

Fig. 16. The effect of pipe material and unsupported length on the maximum flexural stress.

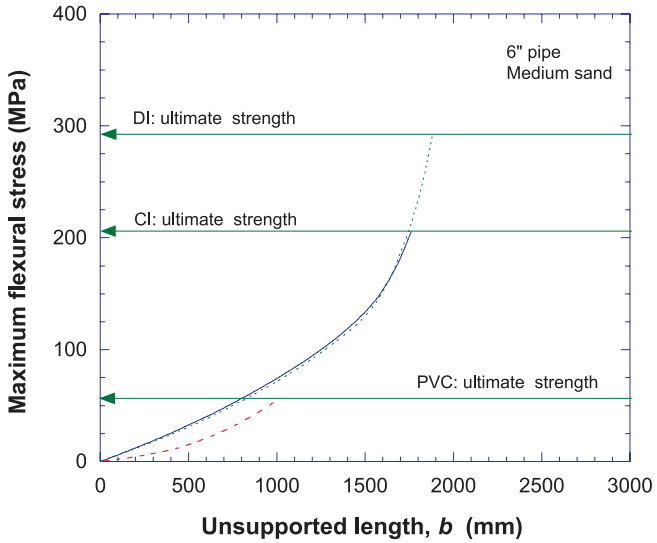

Fig. 17. The effect of soil type on flexural stress.

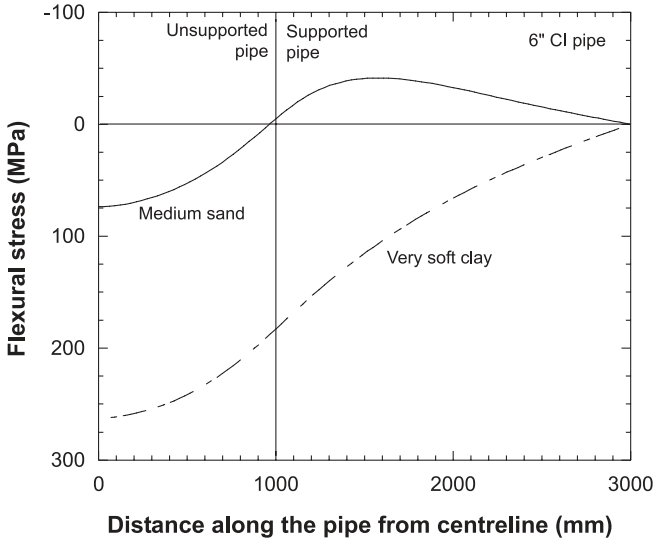

Fig. 18. The effect of soil stiffness on flexural stress.

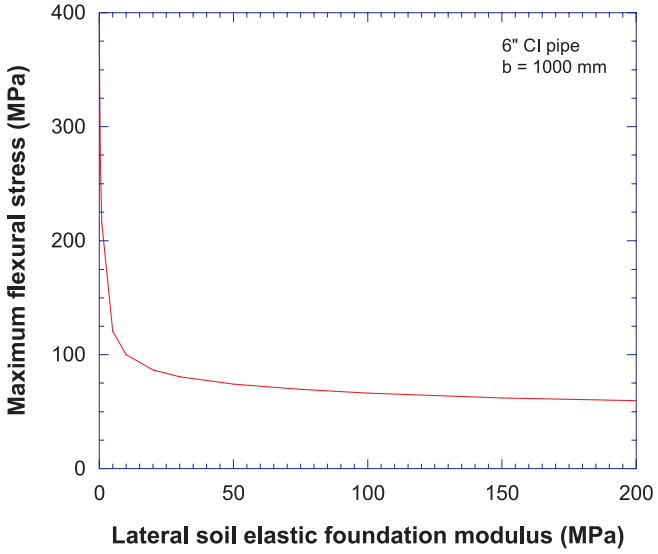

and 52 MPa for medium sand and between 0.08 and 0.55 MPa for very soft clay. The flexural responses (Fig. 17) of the same pipe but buried in different soil types can be dramatically different. This difference in response is further demonstrated in Fig. 18, where the flexural stresses decrease with an increase in k_s'. The pipe effectively behaves like a simply supported beam when k_s' is very small. The flexural stress response does not change (Fig. 18) significantly, however, when the lateral foundation modulus exceeds 50 MPa.

The role of elastoplastic behaviour of the soil on flexural bending stress is shown in Fig. 19 for a pipe with an unsupported length of b = 1000 mm. It can be seen that slightly higher bending stresses are obtained when the bedding is modelled as an elastoplastic medium. The soil near unsupported pipe develops plastic deformations as the unsupported length or overburden load increases. Though the sensitivity analysis does not show a dramatic difference in response, it can be significant to conduct elastoplastic pipe–soil interaction analysis for flexural behaviour, depending on the specific design variables.

Circumferential (or hoop) pipe–soil interaction

It was stated earlier that it is appropriate to consider most common pipe materials as rigid, for pipe sizes of interest in the water industry. The overburden (earth) load together with traffic and frost loads induce thrust and moment in the pipe in the circumferential (or hoop) direction. The rigid-pipe assumption considers there is no interaction support from the soil, and there is zero lateral earth pressure (K_o = 0). This assumption will assure conservative results for the CI pipes and very conservative results for the PVC pipes. The hoop stress, σ_θ^w, for the overburden loads, q (combination of earth, traffic, and frost load), is

Fig. 19. The effect of soil elastoplasticity on flexural stress.

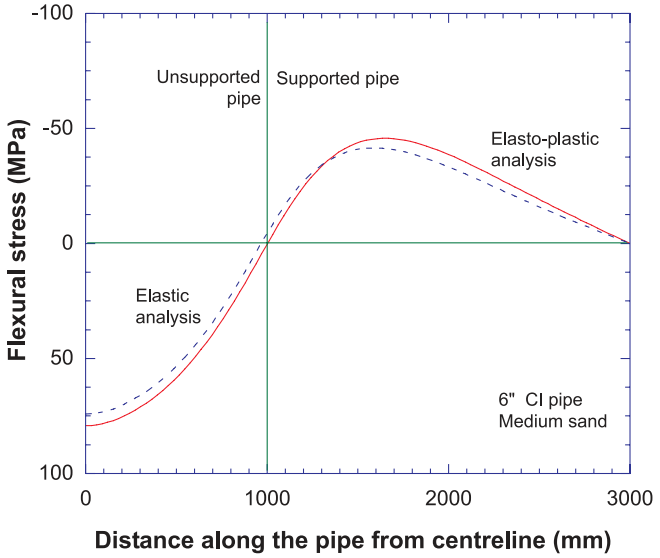

$$[28] \quad \sigma_\theta^{w} = q\left(\frac{3D}{\pi t^2}\right)$$

(Watkins and Anderson 1999).

The hoop stress ($\sigma_\theta^{P_i}$) in a thin pipe as a result of the internal pressure is given by

$$[29] \quad \sigma_\theta^{P_i} = (P_i - P_e)\left(\frac{D-t}{2t}\right)$$

where P_e is the external radial pressure. The radial displacement is constrained by the radial stiffness of the surrounding soil, and the force–displacement relation for a pipe in an infinite medium is given by

$$[30] \quad P_e = k_r^\theta u_r = \frac{E_s}{(D/2)(1+\upsilon_s)} u_r$$

where k_r^θ is the radial soil stiffness, and u_r is the radial displacement. There is no radial restraint in the region where the pipe is unsupported, and hence $P_e = 0$. It is assumed that for the typical radial displacement, the soil remains in the elastic range.

As a consequence of the Poisson's effect on longitudinal stress, the bending hoop stress σ_θ^f is

$$[31] \quad \sigma_\theta^f = -\upsilon_p \sigma_x^f = -\upsilon_p\left(\frac{M_x D}{2I_{zz}}\right)$$

where σ_x^f is the stress in the longitudinal direction due to flexural action. The temperature differential (ΔT) between the inside of the pipe and the surrounding soil induces a thermal hoop stress σ_θ^T:

$$[32] \quad \sigma_\theta^T = \frac{\alpha_p E_p \Delta T}{2(1-\upsilon_p)\ln(r_o/r_i)} \times \left[1 - \ln\frac{r_o}{r} - \frac{r_i^2}{(r_o^2 - r_i^2)}\left(1 + \frac{r_o^2}{r^2}\right)\ln\left(\frac{r_o}{r_i}\right)\right]$$

Fig. 20. Variation of hoop stress, $\sigma_\theta^{P_i}$, with D/t and E_p/E_s for cast iron pipes.

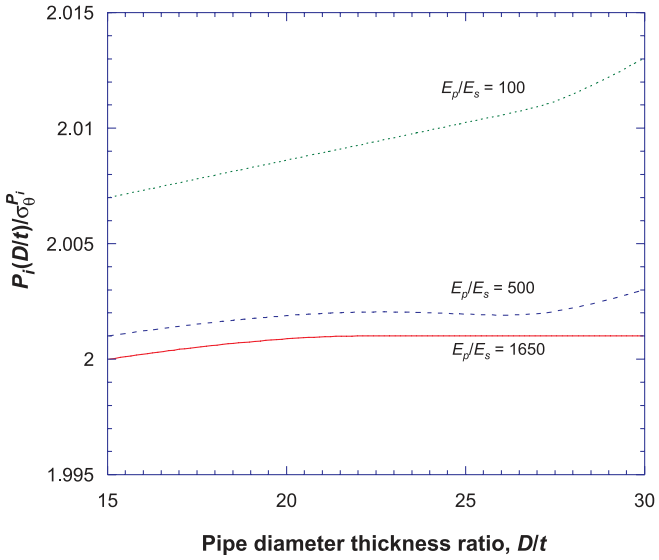

Fig. 21. Variation of hoop stress with change in soil temperature close to the pipe.

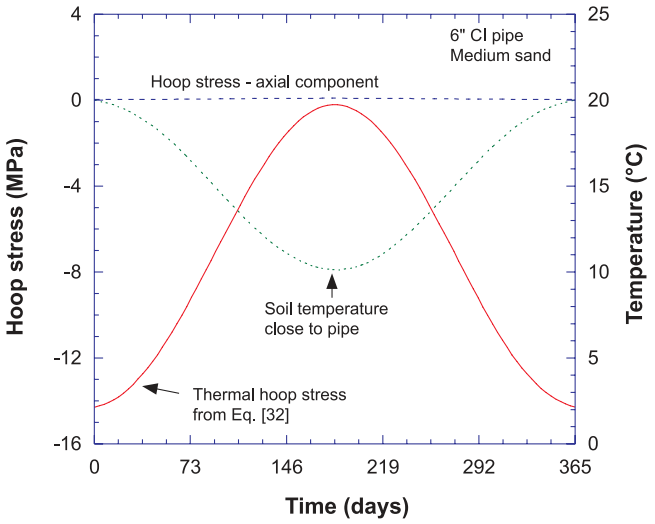

where r_i is the distance from the centre of the pipe to the inner wall, r_o is the distance from the centre of the pipe to the outer wall, and r is the distance from the centre of the pipe to any point (Ugural and Fenster 1987).

The total hoop stress because of external loads, internal pressure, temperature differential, and longitudinal bending is

$$[33] \quad \sigma_\theta^{Total} = \sigma_\theta^{w} + \sigma_\theta^{P_i} + \sigma_\theta^{T} + \sigma_\theta^{f} = \sigma_\theta^{w} + \sigma_\theta^{P_i} + \sigma_\theta^{T} - \nu_p \sigma_x^{f}$$

Sensitivity analyses: hoop stress

The nondimensional form of hoop stress derived using eq. [29] for CI is shown in Fig. 20 (similar plots for PVC and DI were provided by Rajani et al. 1996). Unlike for PVC and DI pipes, the analyses show that CI pipes exhibit little sensitivity to the surrounding soil stiffness, which is altogether not surprising because CI pipes are considered as rigid.

Table 2. Longitudinal stress components from axial and flexural responses.

Domain	Internal pressure	Temperature	Unsupported pipe length	External load	Pipe–soil interaction
$(b + d) \le x < (b + d + f)$	—	—	$\frac{M_x D}{2I_{zz}}$	$\upsilon_p \left(\frac{3D}{\pi t^2}\right) q$	$\frac{F_x}{t}(x_f - f)$
$b < x < (b + d)$	$\chi_2 P_i$	$\chi_3 E_p \alpha_p \Delta T$	$\frac{M_x D}{2I_{zz}}$	$\upsilon_p \left(\frac{3D}{\pi t^2}\right) q$	$\chi_1 E_p \frac{\partial u_d}{\partial x}$
$x < b$	$\chi_2 P_i \left(\frac{\chi_5}{\chi_4}\right)$	$\frac{\chi_6}{\chi_4} E_p \alpha_p \Delta T$	$\frac{M_x D}{2I_{zz}}$	—	$\frac{-2F_x d}{t\chi_4}$

Table 3. Hoop stress components from axial, flexural, and circumferential responses.

Domain	$x > b$	$x \le b$
Unsupported pipe length	$\upsilon_p \frac{M_x D}{2I_{zz}}$	$\upsilon_p \frac{M_x D}{2I_{zz}}$
External load	$\left(\frac{3D}{\pi t^2}\right) q$	—
Internal pressure	$\left(\frac{D-t}{2t}\right) P_i \left\{1 - \frac{\beta_2}{\beta_1} - \upsilon_p E_s \chi_2 \frac{\exp(-\gamma x'') + \exp(\gamma x'')}{\beta_1 \chi_1 E_p (1 + \upsilon_s)[\exp(-\gamma f) + \exp(\gamma f)]}\right\}$	$P_i \left(\frac{D-t}{2t}\right)$
Temperature	$\left(\frac{D}{2t}\right) \alpha_p \Delta T \left\{-E_p \frac{\eta}{\beta_1} + \upsilon_p E_s \chi_3 \frac{\exp(-\gamma x'') + \exp(\gamma x'')}{\beta_1 \chi_1 (1 + \upsilon_s)[\exp(-\gamma f) + \exp(\gamma f)]}\right\}$	$\frac{\alpha_p E_p \Delta T}{2(1 - \upsilon_p) \ln(r_o/r_i)}$
	$+ \frac{\alpha_p E_p \Delta T}{2(1 - \upsilon_p) \ln(r_o/r_i)} \left[1 - \ln \frac{r_o}{r_i} - \frac{r_i^2}{r_o^2 - r_i^2}\left(1 + \frac{r_o^2}{r^2}\right) \ln\left(\frac{r_o}{r_i}\right)\right]$	$\times \left[1 - \ln \frac{r_o}{r} - \frac{r_i^2}{r_o^2 - r_i^2}\left(1 + \frac{r_o^2}{r^2}\right) \ln\left(\frac{r_o}{r_i}\right)\right]$

The effect of temperature on hoop stress is a combination of the radial restraint and the thermal difference between the inside and outside surfaces of the pipe (eq. [32]). As depicted in Fig. 21, the radial restraint is almost zero, whereas the thermal stress calculated using eq. [32] is significant (and in compression). The reason for this is that when the inside temperature is greater than the outside pipe temperature, the hoop stress on the outer surface is negative (compressive).

Conclusions

Current structural design of new water mains is based primarily on circumferential (hoop) stresses imposed by internal pressure and external loads. This design process is valid as long as the pipe is uniformly supported along its length. The deterioration (corrosion) of water mains with time, however, dictates that axial and flexural (longitudinal bending) responses should be considered together with the circumferential response. Furthermore, Rajani et al. (1996) showed the importance of considering temperature differential on the axial response to explain the increased number of water main breaks during periods of late spring – early winter and late winter – early spring, i.e., when the temperature difference between the water and the soil–backfill close to the pipe is likely to be the highest.

In most cases a combination of circumstances leads to the failure of any one particular water main, and it is very difficult to ascertain the precise cause because all the operational data are not always known, e.g., surge pressure, pipe condition, unsupported length, pit geometry. There is a high degree of uncertainty associated with all the factors contributing to pipe failure because of the great spatial variability (even in a moderate size network), especially with corrosion rates. The analytical procedures developed here for jointed water mains and in combination with those developed earlier provide a means to identify the impact of different intervening variables on axial, flexural, and circumferential stress responses. The contributions towards these stress responses from internal water pressure, temperature differential, unsupported pipe length, external loads, and pipe–soil interaction are summarized in Tables 2 and 3.

Sensitivity analyses indicate that the extent of the unsupported length developed as a result of scour has a significant influence on the flexural pipe–soil response, but the axial pipe–soil response is not negatively affected in terms of higher stress. In general, plastic pipes tolerate less loss of support than metallic pipes. In most practical situations, it is appropriate to ignore soil elastoplasticity, since its influence on pipe response is minor.

The physical deterministic model as described in this paper can be used to conduct postfailure analysis. As previously mentioned, there is a high degree of uncertainty associated with all the factors contributing to pipe failure because of the great spatial variability. The physical deterministic model for pipe–soil interaction proposed here

provides point estimates (or fixed values) to determine the factor of safety, which is generally not sufficient. Therefore, the model requires further development to include uncertainties so that the probability of pipe failures at a given time can be quantified to plan maintenance and repair strategies. Possible approaches to do this are Monte Carlo simulations (Sadiq et al. 2004) and fuzzy-based methods (Guynnet et al. 2000) to evaluate the time-dependent reliability, i.e., hazard function of time to failure of buried pipes, and to identify key modelling and input parameters that contribute to the reduction in factor of safety.

References

Committee on Gas and Liquid Fuel Lifelines. 1984. Guidelines for the seismic design of oil and gas pipeline systems. America Society of Civil Engineering, New York.

Das, B.M. 1995. Principles of foundation engineering. PWS Publishing Company, Toronto, Ont.

Guynnet, D.G., Come, B., Perrochet, P., and Parriaux, A. 2000. Comparing two methods for uncertainty in risk assessments. Journal of Environmental Engineering, ASCE, **125**(7): 660–666.

Hetényi, M. 1946. Beams on elastic foundations. University of Michigan Press, Ann Arbor, Mich.

Makar, J. 1999. Diagnostic techniques for sewer systems. Journal of Infrastructure Systems, **5**(2): 69–78.

Makar, J.M., and Rajani, B.B. 2000. Gray cast-iron water pipe metallurgy. Journal of Materials in Civil Engineering, ASCE, **12**(3): 245–253.

Poulos, H.G., and Davis, E.H. 1980. Pile foundation analysis and design. John Wiley and Sons, Toronto, Ont.

Rajani, B., and Zhan, C. 1996. On the estimation of frost loads. Canadian Geotechnical Journal, **33**: 629–641.

Rajani, B., Zhan, C., and Kuraoka, S. 1996. Pipe–soil interaction analysis of jointed water mains. Canadian Geotechnical Journal, **33**: 393–404.

Rowe, R.K., and Davis, E.H. 1982. The behaviour of anchor plates in clay. Géotechnique, **32**: 9–23.

Sadiq, R., Rajani, B., and Kleiner, Y. 2004. Probabilistic risk analysis of corrosion associated failures in cast iron water mains. Reliability Engineering & System Safety, **86**(1): 1–10.

Scott, R.F. 1981. Foundation analysis. Prentice Hall Inc., Englewood Cliffs, N.J.

Trautmann, C.H., O'Rourke, T.D., and Kulhawy, F. 1985. Uplift force–displacement response of a buried pipe. Journal of Geotechnical Engineering, ASCE, **111**(9): 1061–1076.

Ugural, A.C., and Fenster, S.K. 1987. Advanced strength and applied elasticity. Elsevier, New York.

Vesic, A.S. 1961. Bending of beams resting on isotropic elastic solid. Proceedings of the American Society of Civil Engineers, **87**(EM2): 35–51.

Watkins, R.K., and Anderson, L.R. 1999. Structural mechanics of buried pipes. CRC Press, New York.

Appendix A

For a medium-length beam, the governing equations given in eq. [8] and the corresponding derivatives are as follows:

$$v_e = \exp(\lambda x_e)(E_1 \cos \lambda x_e + E_2 \sin \lambda x_e) + \exp(-\lambda x_e)(E_3 \cos \lambda x_e + E_4 \sin \lambda x_e)$$

$$v_e' = \lambda\{\exp(\lambda x_e)[E_1(\cos \lambda x_e - \sin \lambda x_e) + E_2(\cos \lambda x_e - \sin \lambda x_e)] - \exp(-\lambda x_e)[E_3(\cos \lambda x_e + \sin \lambda x_e) - E_4(\cos \lambda x_e - \sin \lambda x_e)]\}$$

$$v_e'' = 2\lambda^2[-\exp(\lambda x_e)(E_1 \sin \lambda x_e - E_2 \cos \lambda x_e) + \exp(-\lambda x_e)(E_3 \sin \lambda x_e - E_4 \cos \lambda x_e)]$$

$$v_e''' = 2\lambda^3\{-\exp(\lambda x_e)[E_1(\cos \lambda x_e + \sin \lambda x_e) - E_2(\cos \lambda x_e - \sin \lambda x_e)] + \exp(-\lambda x_e)[E_3(\cos \lambda x_e - \sin \lambda x_e) + E_4(\cos \lambda x_e + \sin \lambda x_e)]\}$$

It is assumed that because of the bell and spigot connection the vertical displacement and the moment are zero at the finite length of the pipe.

Similarly, at the unsupported beam and the beam supported by a plastic soil connection, to satisfy the continuity, the following boundary conditions are solved at $x = b$ and $x' = 0$:

Condition	Beam resting on plastic foundation	Unsupported beam
$v_c = v_b$	C_1	$\frac{qb^4}{24E_pI_{zz}} + \frac{B_2b^2}{2} + B_4$
$v_c' = v_b'$	C_3	$\frac{qb^3}{6E_pI_{zz}} + B_2b$
$v_c'' = v_b''$	C_2	$\frac{qb^2}{2E_pI_{zz}} + B_2$
$v_c''' = v_b'''$	C_1	$\frac{qb}{2E_pI_{zz}}$

At the intersection of the beam supported by plastic soil and elastic soil, to satisfy the continuity, the following boundary conditions are solved at $x_c = c$ and $x_e = 0$:

Condition	Beam on elastic foundation	Unsupported beam
$v_e = v_c$	$E_1 + E_3$	$\frac{-F_z c^4}{24E_pI_{zz}} + \frac{C_1 c^3}{6} + \frac{C_2 c^2}{2} + C_3 c + C_4$
$v_e' = v_c'$	$\lambda(E_1 + E_2 + E_3 + E_4)$	$\frac{-F_z c^3}{6E_pI_{zz}} + \frac{C_1 c^2}{2} + C_2 c + C_3$
$v_e'' = v_c''$	$-2\lambda^2(E_2 - E_4)$	$\frac{-F_z c^2}{2E_pI_{zz}} + C_1 c + C_2$
$v_e''' = v_c'''$	$2\lambda^3(-E_1 + E_2 + E_3 + E_4)$	$\frac{-F_z c}{E_pI_{zz}} + C_1$

Using the aforementioned governing equations and boundary conditions, the solution can be shown to be

$$B_2 = \frac{F_z c/2E_pI_{zz}\lambda^3 + qb/2E_pI_{zz}\lambda^3 + \theta_3 + \theta_2 + \alpha_6 - \alpha_4}{-\theta_4 - \theta_1 + \alpha_7 - \alpha_5}$$

$$B_4 = C_4 - \frac{qb^4}{24E_pI_{zz}} - \frac{B_2 b^2}{2}$$

$$E_1 = \theta_3 + \theta_4 B_2$$

$$E_2 = \alpha_4 + \alpha_5 B_2$$

$$E_3 = -\theta_2 - \theta_1 B_2$$

$$E_4 = \alpha_6 + \alpha_7 B_2$$

$$C_1 = \frac{qb}{2E_pI_{zz}}$$

$$C_2 = \frac{qb^2}{2E_pI_{zz}} + B_2$$

$$C_3 = \frac{qb^2}{2E_pI_{zz}} + B_2 b$$

$$C_4 = (E_1 + E_3) + \frac{F_z c^4}{24E_pI_{zz}} - \frac{C_1 c^3}{6} - \frac{C_2 c^2}{2} - C_3 c$$

where α_4, α_5, α_6, and α_7 are

$$\alpha_4 = \frac{F_z c}{24E_pI_{zz}\lambda^3}(-c^2\lambda^2 - 3c\lambda - 3) + \frac{qb}{24E_pI_{zz}\lambda^3} \times (3 + 3c^2\lambda^2 + 6c\lambda + 3bc\lambda^2 + 3b\lambda + b^2\lambda^2)$$

$$\alpha_5 = \frac{c}{4\lambda} + \frac{b}{4\lambda} + \frac{1}{4\lambda^2}$$

$$\alpha_6 = \frac{F_z c}{24E_pI_{zz}\lambda^3}(-c^2\lambda^2 + 3c\lambda - 3) + \frac{qb}{24E_pI_{zz}\lambda^3} \times (3 + 3c^2\lambda^2 - 6c\lambda + 3bc\lambda^2 - 3b\lambda + b^2\lambda^2)$$

$$\alpha_7 = \frac{c}{4\lambda} + \frac{b}{4\lambda} - \frac{1}{4\lambda^2}$$

and θ_1, θ_2, θ_3, and θ_4 are

$$\theta_1 = \frac{\alpha_5 \exp(2\lambda e) + \alpha_7(1 - 2\cos^2 \lambda e)}{2\cos \lambda e \sin \lambda e}$$

$$\theta_2 = \frac{\alpha_4 \exp(2\lambda e) + \alpha_6(1 - 2\cos^2 \lambda e)}{2\cos \lambda e \sin \lambda e}$$

$$\theta_3 = \theta_2 \exp(-2\lambda e) - \alpha_4 \tan \lambda e - \alpha_6 \exp(-2\lambda e) \tan \lambda e$$

$$\theta_4 = \theta_1 \exp(-2\lambda e) - \alpha_5 \tan \lambda e - \alpha_7 \exp(-2\lambda e) \tan \lambda e$$

List of symbols

A_T	temperature amplitude
b	unsupported pipe length
B_i^a, C_i^a, D_i^a, F_i^a	axial pipe–soil interaction constants (i = 1, 2)
c	extent of soil in elastoplastic state (lateral)
d	extent of soil in elastic state (axial)
D	outside pipe diameter
e	extent of soil in elastic state
E_i	flexural pipe–soil interaction constants (i = 1–4)
E_p	elastic modulus of pipe
E_s	elastic modulus of soil
f	extent of soil in elastoplastic state (axial)
f_{frost}	frost load factor
F_x	ultimate axial soil resistance
F_z	maximum lateral soil resistance per unit length
G_s	soil shear modulus
H	burial depth of water mains
I_{zz}	pipe second moment of inertia around the z axis
k_r^θ	radial soil stiffness
k_s^a	axial pipe–soil reaction modulus
k_s'	lateral soil elastic foundation modulus
K_o	coefficient of active resistance at rest
L	half jointed pipe length
M_x	bending moment
N_z	dimensionless resistance factor for sand
N_c	bearing capacity type factor for clay
P_e	external radial pressure
P_i	pipe internal pressure
q	overburden load
Q	shear force

r distance from the centre of the pipe to any point
r_i distance from the centre of the pipe to the inner wall
r_o distance from the centre of the pipe to the outer wall
s_u undrained shear strength of clay
t pipe wall thickness
u axial displacement
u_b, u_b' pipe axial displacement and strain in the unsupported region
u_d, u_d' pipe axial displacement and strain in the elastic region
u_f, u_f' pipe axial displacement and strain in the elastoplastic region
u_r pipe radial displacement
u_x soil displacement at ultimate axial resistance
v vertical displacement
v_b, v_b', v_b'', v_b''' pipe vertical displacement, slope, curvature and change in curvature in the unsupported region
v_c, v_c', v_c'', v_c''' pipe vertical displacement, slope, curvature and change in curvature in the elastoplastic region
v_e, v_e', v_e'', v_e''' pipe vertical displacement, slope, curvature and change in curvature in the elastic region
v_u soil displacement at the ultimate lateral resistance
x distance along pipe from the centreline
x_b, x_c, x_d, x_e, x_f longitudinal coordinate systems for axial (Fig. 4) and lateral (Fig. 11) pipe-soil interaction
α adhesion coefficient
α_i flexural pipe–soil interaction constants (i = 4–7)
α_p linear thermal expansion coefficient of pipe material
β_l axial pipe–soil interaction constants
δ frictional angle between pipe material and surrounding backfill
ΔT maximum temperature difference between water and surrounding soil
ϕ soil internal friction angle
γ reciprocal of the axial characteristic length
γ_s soil submerged unit weight
η ratio of elastic pipe and soil properties as defined by Rajani et al. (1996)
λ reciprocal of the flexural characteristic length
υ_s Poisson's ratio of soil
υ_p Poisson's ratio of pipe
θ slope
θ_i flexural pipe–soil interaction constants (i = 1–4)
ρ unit density soil
σ_x^a axial stress
σ_x^f stress in longitudinal direction due to flexural action
$\sigma_\theta^{P_i}$ hoop stress due to internal pressure
σ_θ^f hoop stress due to the Poisson's effect of longitudinal bending
σ_θ^T hoop stress due to temperature differential
σ_θ^{Total} total hoop stress
σ_θ^w hoop stress due to overburden loads
χ_i axial pipe–soil interaction constants (i = 1–6)